JOURNAL of the MEXICAN CHEMICAL SOCIETY

https://www.jmcs.org.mx/

Article

Open Access

J. Mex. Chem. Soc. **2026**, *70(1):e2440*

Received February 9th, 2025
Accepted December 9th, 2025

http://dx.doi.org/10.29356/jmcs.v70i1.2440
e-location ID: 2440

Keywords:
Molecular dynamics; CBD; alginate; encapsulation

Palabras clave:
Dinámica molecular; CBD; alginato; encapsulación

***Corresponding author:**
Lucero Rosales-Marines
email: lucero_rosales@uadec.edu.mx
Phone: + 52 844-235-4606

ISSN-e 2594-0317

Molecular Dynamics Study to Analyze the Interactions between Sodium Alginate and CBD

Erik De La Rosa-Montelongo, Lucero Rosales-Marines*, Lorena Farías-Cepeda, Juan De La Peña-Zúñiga

Facultad de Ciencias Químicas, Universidad Autónoma de Coahuila, Saltillo, Coahuila, México.

Abstract. Sodium alginate is a hydrophilic polysaccharide, widely recognized for its biocompatibility, making it suitable for applications in the human body. Its growing use as a matrix for encapsulating hydrophobic molecules and in controlled drug release highlights its research potential. Cannabinoids, on the other hand, are generally hydrophobic; cannabidiol (CBD) stands out for its therapeutic properties, attracting significant interest in recent years. In this study, molecular dynamics simulations were used to investigate the interactions between sodium alginate and CBD in water and a simulated $CaCl_2$ saline solution to assess their affinity and the potential of alginate as an encapsulation matrix. Both systems were evaluated under identical simulation conditions to observe interactions within the CBD-SA complexes. Molecular parameterization employed the OPLS-AA force field, with simulations running for 100 ns. The results revealed significant interactions in saline and aqueous environments, with differences suggesting the optimal physiological medium for CBD encapsulation. Overall, sodium alginate showed limitations in fully encapsulated CBD due to inconsistent interactions, although cases are highlighted where alginate combined with other compounds showed promising results.

Resumen. El alginato de sodio, es un polisacárido hidrofílico, ampliamente reconocido por su biocompatibilidad, lo que lo hace adecuado para aplicaciones en el cuerpo humano. Su creciente uso como matriz para encapsular moléculas hidrofóbicas y en la liberación controlada de fármacos destaca su potencial de investigación.

J. Mex. Chem. Soc. **2026**, *70(1):e2440*
Regular Issue

ISSN-e 2594-0317

Los cannabinoides, en cambio, son generalmente hidrofóbicos; el cannabidiol (CBD) sobresale por sus propiedades terapéuticas, atrayendo gran interés en los últimos años. En este estudio, se usaron simulaciones de dinámica molecular para investigar las interacciones entre el alginato de sodio y el CBD en agua y en una solución salina simulada de $CaCl_2$, con el fin de evaluar su afinidad y el potencial del alginato como matriz para la encapsulación. Ambos sistemas fueron evaluados bajo condiciones de simulación idénticas para observar interacciones en los complejos CBD-SA. La parametrización molecular utilizó el campo de fuerza OPLS-AA y las simulaciones se realizaron durante 100 ns. Los resultados revelaron interacciones significativas en entornos salino y acuoso, con diferencias que sugieren el medio fisiológico óptimo para la encapsulación de CBD. En general, el alginato de sodio mostró limitaciones para encapsular completamente el CBD debido a interacciones inconsistentes, aunque se destacan casos donde el alginato combinado con otros compuestos mostró resultados prometedores.

Introduction

In recent years, cannabinoids have gained interest due to their widespread use and therapeutic contributions to various conditions. Among cannabinoids, cannabidiol (CBD) stands out for its pharmacological effects and is a promising candidate for advanced therapeutic applications, such as in cancer conditions, neuropathies, rheumatoid arthritis, etc. [1–3]. However, CBD has disadvantages that reduce its bioavailability for use as an effective treatment. This is due to its easy oxidation when exposed to light and its high hydrophobicity [4]. Therefore, complete or partial isolation is used to eliminate these drawbacks through encapsulation, thus providing additional properties such as hydrophilicity and selectivity.

There are different types of nanomaterials or nanocarriers used for isolating CBD. Among the most prominent for encapsulating CBD are those with a lipid base, such as emulsions, vesicles, and lipid nanoparticles. These lipid-based nanocarriers achieve the highest encapsulation percentages, with almost 100 % efficiency. However, polymeric and hybrid nanocarriers have also been used for isolation. Although their encapsulation percentages are lower, some matrices have shown good results [5]. For example, Wang et al. encapsulated CBD using a matrix made of zein and whey protein, forming nanoparticles that carried CBD at 0.6 % w/w. They achieved an encapsulation efficiency of 86 % and stability for up to three weeks, obtaining favorable results in preserving the antioxidant properties of CBD through encapsulation in zein-whey protein nanoparticles [6].

Polysaccharides are used for the encapsulation of various drugs for controlled release, as they are natural, biodegradable, and biocompatible polymers. Examples include chitosan, chitin, carrageenan, collagen, cyclodextrins, alginates, among others [7]. Among the polysaccharides used for CBD encapsulation are chitosan, alginates, and cyclodextrins (CD). For example, a matrix of sodium alginate (SA) and chitosan has been used to formulate capsules that provided an encapsulation efficiency of 87 %. However, Villate et al.'s study presented a reduction in the cost of the CBD encapsulation process compared to the use of other matrices [8].

On the other hand, there are theoretical studies using molecular simulation, specifically molecular dynamics (MD). For example, among these studies, one employed MD to analyze the interactions between phenolic compounds and alginate chains, concluding that the predominant interaction occurs through hydrogen bonding. This interaction was investigated with the aim of utilizing alginate for the removal of phenolic contaminants from water bodies [9]. Similarly, molecular dynamics simulations have been used to study the interactions between a single polyguluronate chain and mono- and divalent metal cations (Na^+, K^+, Mg^{2+}, and Ca^{2+}), revealing that the chain conformation and hydrogen bonding were largely insensitive to the surrounding anionic charge, while also showing a higher affinity of alginate for divalent cations [10].

A study conducted using MD to evaluate the energetic, thermodynamic aspects, and interactions between the CDs (α, β, and γ) and CBD is that of da Silva et al. [11], this was done to form a complex and determine which CD would be the best matrix for encapsulating CBD, while observing the influence of temperature during complex formation. This research was carried out using GROMACS. Upon completing their analysis, they found that the matrix showing the best receptor properties for encapsulating CBD was γ-CD.

While the importance of a theoretical study using simulation lies in achieving a better understanding of the energy, interactions, and thermodynamics of the system, it is also useful for establishing the optimal

J. Mex. Chem. Soc. **2026**, *70(1):e2440*
Regular Issue

ISSN-e 2594-0317

conditions for conducting the experimental part. From this perspective, theoretical studies serve as a reference for experimental studies, helping to predict the best parameters for achieving encapsulation [12].

In this context, sodium alginate (SA) emerges as a potential alternative for CBD encapsulation. This polysaccharide has proven to be effective in the isolation and controlled release of various drugs [13]. The present study aimed to evaluate the potential use of sodium alginate as a matrix for CBD, leveraging its inherent advantages from a theoretical perspective using MD techniques to observe the interaction energy between SA and CBD in different environments, thereby determining how optimal it is.

Materials and methods

The structures of CBD (CID 644019) and SA (CID 5102882) were obtained in SDF format from the PubChem database (https://pubchem.ncbi.nlm.nih.gov/). Preliminary tests were conducted using alginate chains of shorter length, starting with three monomers and progressively increasing the number. The final choice of a seven-monomer chain was because alginate does not possess a single well-defined structure but rather exhibits variability in both conformation and size. Therefore, this length was considered a reasonable minimum for conducting molecular dynamics simulations. This decision was supported by previous studies in literature, where models ranging from three to twenty-seven monomers have been simulated [14,15].

To construct the three-dimensional model of sodium alginate (SA), a linear sequence composed of seven monomeric units was designed: four units of α-L-guluronic acid (G) and three units of β-D-mannuronic acid (M), arranged in a GMG pattern. The initial molecular structure was built and adjusted using the Avogadro program [16], resulting in alginic acid (alginate after deprotonation of the carboxyl groups). To neutralize the resulting negative charges, seven Na^+ ions were added to the system. The conversion from SDF format to PDB format was performed using version 2.3.1 of OpenBabel [17] to elongate the SA chain and parameterize both molecules with the OPLS-AA force field, which was generated using the LigParGen Server [18–20]. The OPLS-AA force field was chosen for this study due to its broad validation in the literature for simulating organic and biomolecular systems. Previous studies have demonstrated that OPLS-AA can accurately reproduce experimental observables such as binding free energies, solubility changes, and temperature-dependent conformational behaviors [21,22]. The initial configuration of the alginate–CBD system was obtained using AutoDock Tools through a molecular docking approach, which allowed for the definition of the starting positions of both molecules. Following docking, the system was parameterized using the force field for subsequent molecular dynamics simulations [23,24]. Once the SA was parameterized, 7 Na^+ ions were introduced to compensate for the negative charge resulting from the deprotonation of the carboxyl group, all using version 2024 of GROMACS [25]. Both molecules (CBD-SA) were combined into a single file in GRO format to create the corresponding systems. The simulated system consists of one CBD molecule and one alginate molecule. A single molecule of each component was used to observe their individual interaction behavior and mutual affinity. While in a real system the number of molecules would be significantly higher, this approach allows for the isolated evaluation of non-covalent interactions between both components, as well as for studying how variations in concentration and temperature may impact the stability of the system. Fig. 1 displays the complex formed with the considerations in a three-dimensional structure.

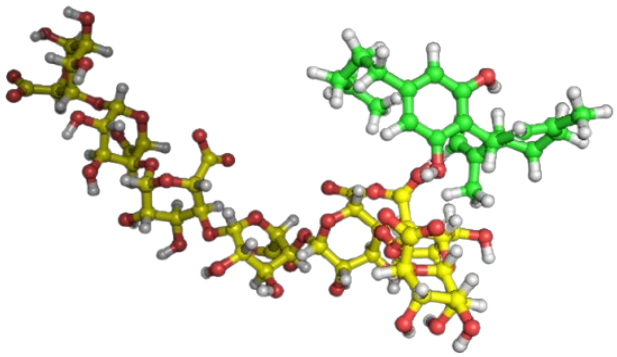

Fig. 1. Complex is formed by an alginate molecule (carbon: yellow, oxygen: red, hydrogen: white) and a CBD molecule (carbon: green, oxygen: red, hydrogen: white).

http://dx.doi.org/10.29356/jmcs.v70i1.2440

J. Mex. Chem. Soc. **2026**, *70(1):e2440*
Regular Issue

ISSN-e 2594-0317

Three different systems were considered for analysis: one consisting of the CBD-SA complex submerged only in water (S1), another system of CBD-SA submerged in a 0.8 M $CaCl_2$ saline solution (S2), and a third system of CBD-SA submerged in a 1 M $CaCl_2$ saline solution (S3). For this, the complexes were placed in a cubic box of 138.57 nm^3 for systems S1 and S2, and a second box of 103.82 nm^3 for system S3. The type of water used for all systems was SPC/E, with a minimum distance of 1 nm from the edge of the box and the complexes. The amount of water molecules for system S1 was 4448. The configurations for systems S2 and S3 were as follows: S2 contained 4238 water molecules, 70 Ca^{2+} ions, and 140 Cl^- ions; and for S3, there were 3130 water molecules, 63 Ca^{2+} ions, and 126 Cl^- ions, all while maintaining the charges of the systems to keep them neutralized. The simulation box for system S3 was defined with a smaller volume compared to S1 and S2 to achieve the target ionic concentration. During system preparation, attempts to build S3 using the same box size as the other systems resulted in insufficient effective concentration of Ca^{2+} and Cl^- ions, even after adding the correct number of ions. To resolve this, the volume was reduced to increase the ion density while maintaining appropriate solvation and minimum solute–box edge distances. This adjustment ensured consistency with the intended salinity and did not compromise system integrity. The configuration of the systems is summarized in Table 1.

Table 1. Description of systems.

MD system name	Box	Volume of box (nm^3)	Number of SPC/E Water	Number of Na ions	Number of Ca ions	Number of Cl ions
S1	Cubic	138.57	4448	7	0	0
S2	Cubic	138.57	4238	7	70	140
S3	Cubic	103.87	3130	7	63	126

System minimization was performed using the steepest descent algorithm, and the equilibration phase was conducted with positional restraints to ensure the proper arrangement of the solvent around the complexes. This phase was carried out under NPT conditions (P = 1 bar and T = 300 K), which were applied after a prior NVT equilibration. Both equilibration stages were performed for 1000 ps. To determine the optimal equilibration time, three different relaxation times were tested: 1000 ps (1 ns), 10 ns, and 100 ns. However, the behavior of both temperature and pressure remained consistent across all three durations, indicating that the system had already reached equilibrium at the shortest time. Therefore, a 1000 ps equilibration time was chosen, as it significantly reduced the computational cost while maintaining the reliability of the system's stabilization. This decision was further supported by the analysis of thermodynamic variables and aligns with previous studies involving polymeric systems and small molecules.

Temperature control was achieved using the V-rescale thermostat with a constant time of 0.1 ps, while pressure was controlled using the C-rescale barostat with a relaxation constant of 1 ps, both modified versions of the Berendsen thermostat and barostat [26]. The LINCS (Linear Constraint Solver) algorithm was applied to all bonds within the complex, with small steps of 2 fs [27]. The hydrogen bonds (H-bonds) algorithm was employed to analyze interactions involving water molecules. Hydrogen bonds were identified based on a geometric criterion implemented in the gmx hbond tool of GROMACS. A hydrogen bond was considered to exist when the donor–acceptor distance was less than 0.35 nm and the hydrogen–donor–acceptor angle exceeded 150°, which are standard cutoffs in molecular dynamics simulations. The analysis was performed across the entire trajectory using a continuous time series, allowing the identification of both persistent and transient interactions. Donor and acceptor groups were defined according to the topology files, and only those involving alginate and CBD were included in the final analysis. A cut-off radius of 1 nm was used for non-bonded interactions, and electrostatic interactions were calculated using the Particle Mesh Ewald method.

These stages are crucial as proper minimization and equilibration of the systems allow for production without errors or system collapses. After completing these stages, the corresponding simulations were carried out with the same considerations as the previous phases, with a simulation time of 100 ns. No issues arose during or after the simulations. The parameters and conditions used are summarized in Table 2.

http://dx.doi.org/10.29356/jmcs.v70i1.2440

J. Mex. Chem. Soc. **2026**, *70(1):e2440*
Regular Issue

ISSN-e 2594-0317

Table 2. Description and units of settings and parameters.

Minimization	
Algorithm	Steepest descent
NVT & NPT	
Equilibration time	1000 ps
Thermostat	V-rescale
Temperature	300 K
Time constant (Tτ)	0.1 ps
Barostat	C-rescale
Pressure	1 bar
Time constant (Pτ)	1 ps
Nonbonded settings	
Cut-off scheme	Verlet
Van der Waals	1.0 nm
Electrostatics	1.0 nm
Bond parameters	
Constraint algorithm	LINCS
Constraint	H-Bond
Long Range Electrostatics	PME
Production	
Simulation time	100 ns
Δt	0.2 fs
Cut-off	1.0 nm

The topologies and parameters for CBD and alginate were generated using the LigParGen server with the OPLS-AA force field. All bonded and non-bonded parameters, including atomic charges, dihedral angles, and Lennard-Jones constants, were obtained directly from the server and are provided in Supplementary Information (Table S1 and Table S2).

http://dx.doi.org/10.29356/jmcs.v70i1.2440

J. Mex. Chem. Soc. **2026**, *70(1):e2440*
Regular Issue

ISSN-e 2594-0317

Results and discussion

Fig. 2 shows the evolution of the distance between CBD and SA over time, which is known as root-mean-square deviation (RMSD) and was analyzed for the three systems to assess their stability. Although there is no single effective method to demonstrate the stability of a system, RMSD graphs can serve as a preliminary indicator of stability since they provide valuable information to analyze whether interactions exist between the molecules. These interactions can be of different types, such as hydrogen bonds, Van der Waals forces, electrostatic forces, salt bridges, conformational changes, etc., which could indicate whether the molecules are compatible with each other.

RMSD analysis was performed using the gmx rms tool from GROMACS, aligning each frame of the trajectory with the initial structure through a least-squares fitting procedure. This method allowed the observation of global conformational changes throughout the simulation time. The fluctuations observed in the RMSD plot were interpreted in the context of non-covalent interactions between alginate and CBD. Thus, increases in RMSD may correspond to repulsive interactions or conformational rearrangements, whereas decreases or plateaus may indicate stabilization due to attractive forces such as hydrogen bonding, van der Waals interactions, or electrostatic attractions. These interpretations were supported by complementary analyses, including hydrogen bond monitoring and visual inspection of representative structures along the trajectory.

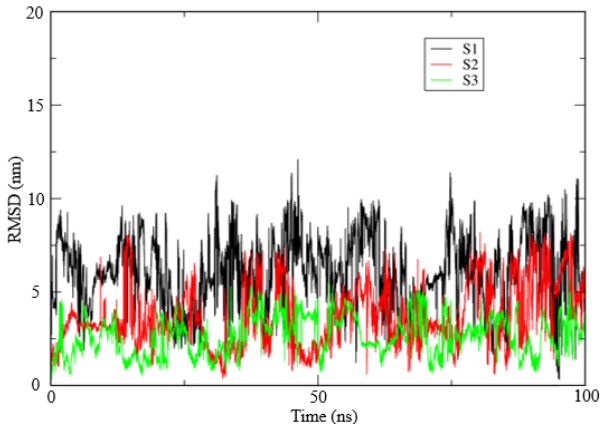

Fig. 2. Comparison of RMSD profiles at different concentrations; S1: Water, S2: 0.8 M $CaCl_2$, S3: 1 M $CaCl_2$.

When analyzing the comparative RMSD graph for the three systems, several fluctuations can be observed, indicating constant movement of the CBD molecule relative to SA. This can be interpreted as the forces of repulsion and attraction between the two molecules. For the first system, which contains only water molecules, these forces are mostly repulsive, while as the salinity of the medium increases, a greater number of attractive forces are observed. However, in the first system, it can be noted that within these fluctuations, there are small intervals where the attractive forces are stronger than the repulsive ones, allowing the CBD to approach the SA. This is represented in Fig. 3, which provides information on the number of hydrogen bond interactions between CBD and SA. Similarly, Van der Waals interactions can be analyzed through the Lennard-Jones (LJ) potential, which quantifies both repulsive and attractive forces between atom pairs. In this work, the total Van der Waals energy reported corresponds to the sum of all LJ interactions between alginate and CBD, providing a global measure of their interaction over time. Instantaneous LJ energy values were extracted using the GROMACS gmx energy tool, integrating all relevant pairs into a single total value per time point. This allows monitoring of the net Van der Waals interactions and facilitates the interpretation of molecular binding or repulsion events. Additionally, Coulomb electrostatic interactions were also examined. These are represented in Figures 4 and 5, where it can be seen how the CBD molecule is attracted by these types of interactions towards SA.

It is important to clarify that RMSD was calculated for the sodium alginate (SA) structure relative to the initial position of the CBD molecule, to monitor the conformational changes of the host matrix throughout the simulation. Focusing on SA allowed us to identify how its structure responded to the presence and proximity of CBD under different environmental conditions. While RMSD provides useful insight into structural dynamics, we

J. Mex. Chem. Soc. **2026**, *70(1):e2440*
Regular Issue

ISSN-e 2594-0317

recognize that it does not represent a direct measure of thermodynamic stability. Therefore, it was used as a qualitative descriptor of molecular behavior, especially when interpreted in conjunction with hydrogen bonding analysis and energy profiles.

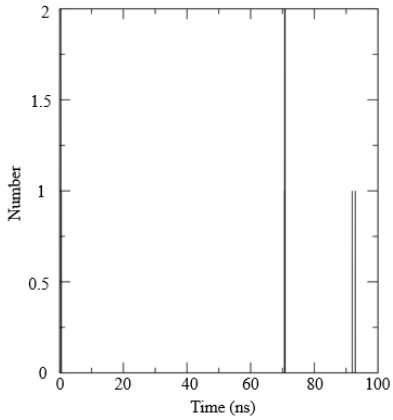

Fig. 3. Hydrogen bonds between SA and CBD; S1.

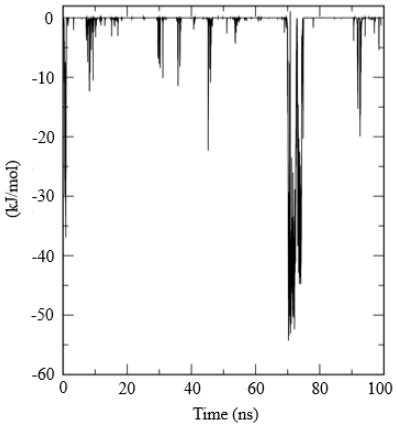

Fig. 4. Lennard-Jones potential between SA and CBD; S1.

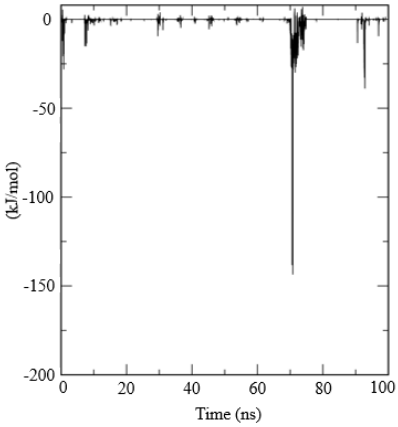

Fig. 5. Coulomb electrostatic forces between SA and CBD; S1.

http://dx.doi.org/10.29356/jmcs.v70i1.2440

J. Mex. Chem. Soc. **2026**, *70(1):e2440*
Regular Issue

ISSN-e 2594-0317

In contrast, for S2, an increase in attractive forces is observed, which leads to a higher number of interactions between CBD and SA, showing more hydrogen bond interactions due to the proximity of the molecules. Likewise, the attractive forces between CBD and SA are better represented by the Lennard-Jones potential and Coulombic electrostatic forces. All these interactions can be seen in Figures 6, 7, and 8, respectively. However, the interactions remain few and do not have a good retention time, suggesting that S2 is still an unstable system for forming the CBD-SA complex.

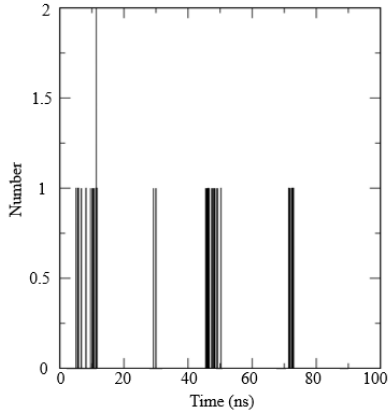

Fig. 6. Hydrogen bonding between SA and CBD; S2.

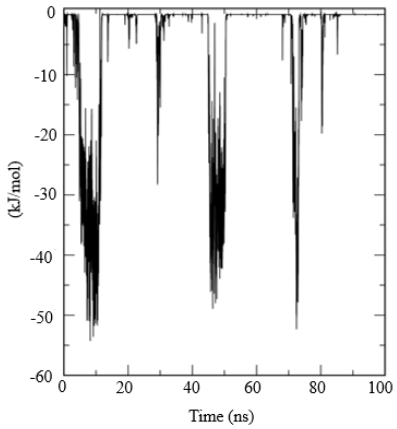

Fig. 7. Lennard-Jones potential between SA and CBD; S2.

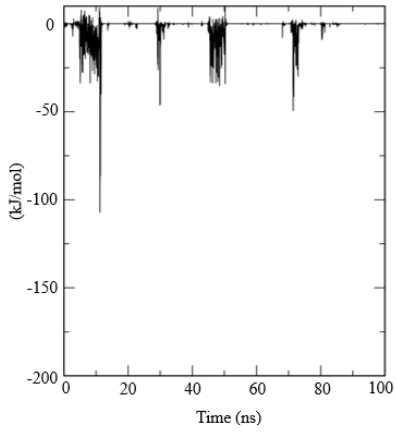

Fig. 8. Coulomb electrostatic forces between SA and CBD; S2.

http://dx.doi.org/10.29356/jmcs.v70i1.2440

J. Mex. Chem. Soc. **2026**, *70(1):e2440*
Regular Issue

ISSN-e 2594-0317

The increase in attractive forces for S2 may be due to the addition of a certain concentration of $CaCl_2$, which enhances the stability of this complex thanks to the presence of more metallic ions in the system. This is consistent with what is shown in the literature, particularly in the study by Da Silva et al., where they concluded not only that the best cyclodextrin for encapsulating CBD is γ-CD but also observed that the γ-CD-CBD complex is better formed in a saline environment. This is because an ion-rich environment facilitates interactions between the CBD and CDs, with the main factors affecting encapsulation being the type of CD and the environment, as temperature did not have a significant effect [11]. Although the increase in this case is not as substantial, it can be said that CBD encapsulation would be more effective in a saline environment. This is more evident for S3, where once again the attractive forces were greater. This is reflected in the increase in hydrogen bonding interactions, Lennard-Jones potential, and Coulomb electrostatic forces, as shown in Figures 9, 10, and 11.

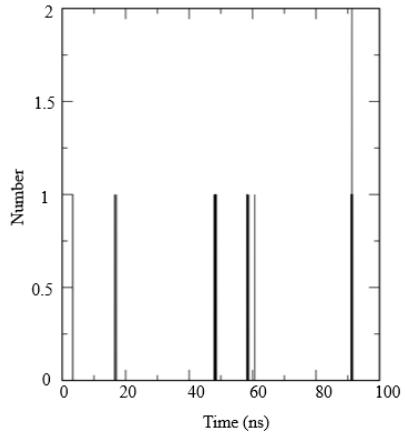

Fig. 9. Hydrogen bonding between SA and CBD; S3.

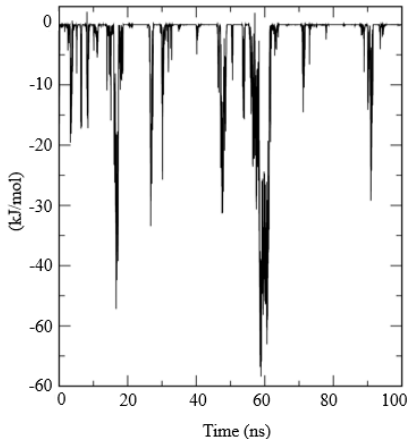

Fig. 10. Lennard-Jones potential between SA and CBD; S3.

http://dx.doi.org/10.29356/jmcs.v70i1.2440

J. Mex. Chem. Soc. **2026**, *70(1):e2440*
Regular Issue

ISSN-e 2594-0317

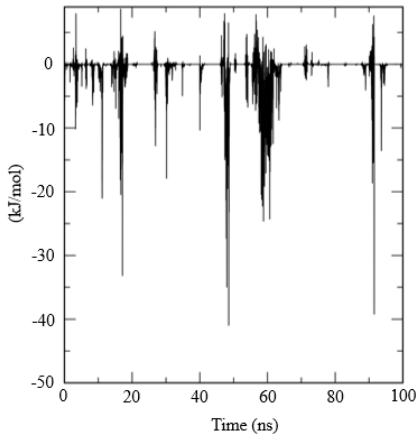

Fig. 11. Coulomb electrostatic forces between SA and CBD; S3.

To determine whether the temperature used in the simulations was a determining factor in the stability of the complex, simulations were conducted at different temperatures. For this purpose, system S3, which showed the greatest stability at 300 K, was selected and evaluated at three additional temperatures (310, 320, and 330 K). The results showed an increase in the stability of the complex when the temperature was raised to 310 K. However, when the temperature was further increased to 320 and 330 K, a decrease in the complex's stability was observed. This could be attributed to the fact that increasing the temperature also increases kinetic energy, which tends to decrease the attractive forces and amplify the repulsive forces. Therefore, the formation of the CBD-CD complex would be more likely to occur at a temperature close to 310 K. This behavior can be observed in Fig. 12, which shows a comparison of the stability of the complexes as the temperature changes. Fig. 13 represents the corresponding interactions of hydrogen bonding for the S3 system at 310 K, to observe the notable increase that occurred with a 10-degree temperature rise.

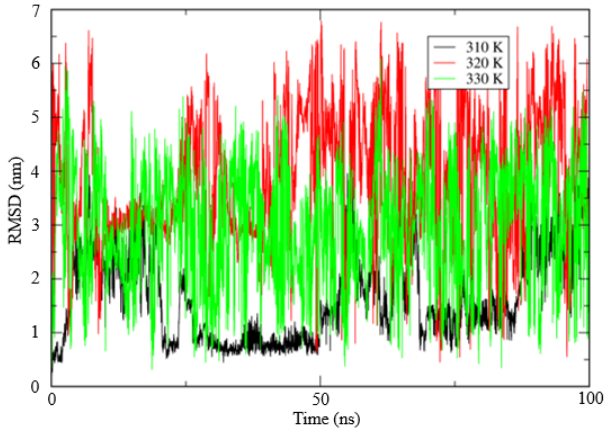

Fig. 12. RMSD profile for S3 at different temperatures.

http://dx.doi.org/10.29356/jmcs.v70i1.2440

J. Mex. Chem. Soc. **2026**, *70(1):e2440*
Regular Issue

ISSN-e 2594-0317

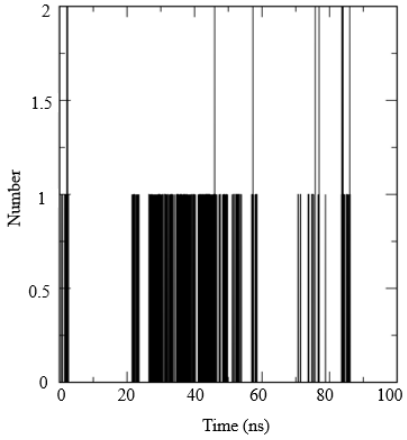

Fig. 13. Hydrogen bonds between SA and CBD; S3 310K.

The results revealed that temperature plays a significant role in promoting non-covalent interactions that contribute to the system's stability. However, it was also observed that increasing the temperature beyond a certain threshold leads to destabilization of the complex. This effect is likely associated with a rise in kinetic energy, which enhances repulsive forces between the molecules. To further explore this behavior, the kinetic and potential energy profiles of the system at different temperatures were analyzed. As shown in Fig. 13, the system exhibited the highest degree of structural stability at 310 K, while temperatures above 320 K resulted in noticeable destabilization. This is further supported by the kinetic energy profile presented in Fig. 14, which reflects the increased molecular motion at elevated temperatures. Additionally, Fig. 15 shows the corresponding potential energy values, highlighting how thermal agitation can disrupt favorable interactions, ultimately reducing the persistence of the CBD–SA complex.

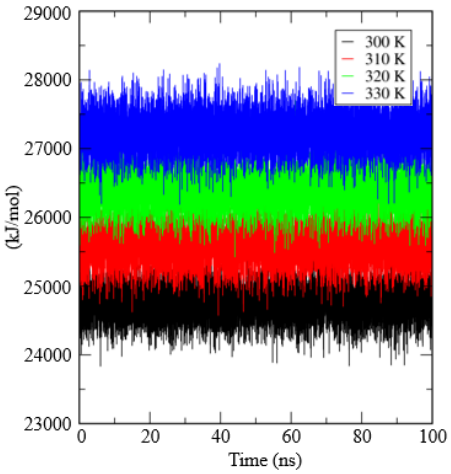

Fig. 14. Kinetic energy for the S3 at different temperatures; 300 K, 310 K, 320 K & 330 K.

http://dx.doi.org/10.29356/jmcs.v70i1.2440

J. Mex. Chem. Soc. **2026**, *70(1):e2440*
Regular Issue

ISSN-e 2594-0317

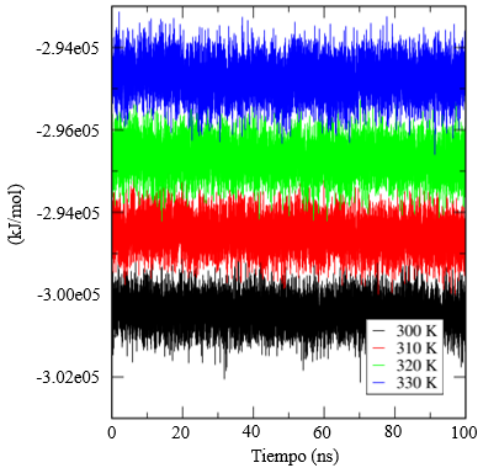

Fig. 15. Potential energy for the S3 at different temperatures.

The previously shown results are consistent with findings in the literature. In an experimental study conducted by Majimbi et al., medium-viscosity SA was used as a matrix to form microcapsules with a 2 % CBD loading. This study highlights the encapsulation percentage obtained, which was only 23 ± 1.2 %, with a particle size of 400 ± 50 μm. Therefore, despite partially encapsulating the molecule, it did not show the desired results as a matrix, leading them to rely on the addition of deoxycholic acid (DCA) capsules to improve the encapsulation percentage [28]. These results support the findings of the present molecular dynamics study, which shows that, although non-covalent interactions such as hydrogen bonding and van der Waals forces do occur between CBD and SA, their intensity and persistence are limited, especially in the absence of crosslinkers or additional polymers. Therefore, the simulations revealed that increased salinity enhances complex stability, while elevated temperatures reduce it, suggesting that environmental conditions are a critical factor. This mechanistic insight helps explain the low encapsulation efficiency observed experimentally and highlights the need for formulation strategies that enhance non-covalent interactions, such as the inclusion of secondary encapsulating agents or polymer blends. Although advanced analytical tools such as radial distribution functions (RDF) or cluster analysis were not applied in this study, the system's structural and energetic behavior was thoroughly characterized using complementary approaches. These included RMSD analysis, hydrogen bond monitoring, Lennard-Jones and Coulombic interaction energies, as well as kinetic and potential energy profiles. This combination of descriptors provided a consistent framework for evaluating the influence of salinity and temperature on the stability of the CBD–SA complex. Future work may incorporate RDF or clustering techniques to gain deeper insights into the spatial distribution of CBD around the alginate structure or to identify potential aggregation behavior. Nevertheless, the current analyses offer a comprehensive qualitative understanding of the non-covalent interactions that govern the encapsulation process.

Conclusions

A 1:1 stoichiometry between CBD and SA was adopted in this study, following approaches used in previously reported methodologies for host–guest systems in molecular dynamics simulations, such as CBD–CD) complexes, where a single molecule of each species is modeled to evaluate the energetic aspects of the interaction in detail. This simplified configuration allows for a detailed and computationally efficient analysis of both molecular and non-molecular interactions, particularly because the encapsulation process is primarily governed by non-covalent forces.

Based on the findings of the present work, effective encapsulation of CBD by SA would require the process to occur in a saline medium, as the presence of metal ions enhances non-covalent interactions between

J. Mex. Chem. Soc. **2026**, *70(1):e2440*
Regular Issue

ISSN-e 2594-0317

the two molecules, thereby improving system stability and promoting complex formation. It was also observed that temperature plays a significant role: interactions increased at 310 K but decreased at higher temperatures due to the increase in kinetic energy. It is important to note that, while a single alginate chain of seven monomers was used for computational feasibility, alginate is a polymer of variable length and conformation that can form crosslinked networks for encapsulation. Although alginate alone may not achieve high encapsulation efficiencies for CBD, as suggested by experimental studies, its performance improves when modified or combined with other polymers such as chitosan. Therefore, the molecular dynamics results suggest that alginate by itself may be insufficient for efficient CBD encapsulation, and that the degree of complexation will largely depend on the salinity of the medium.

It is acknowledged that a single 100 ns trajectory per system does not provide sufficient statistical sampling to estimate uncertainties or reproducibility for dynamic metrics such as RMSD or hydrogen bond counts. However, the aim of this study was to provide a qualitative and mechanistic insight into the molecular interactions between CBD and alginate under varying environmental conditions. Although quantitative conclusions regarding population distributions or statistical significance are beyond the scope of this work, the trends observed across the three modeled systems were consistent and supported by multiple types of interaction analysis (e.g., hydrogen bonding, van der Waals and Coulomb energies, and structural deviations). Future work will focus on replicating these simulations and expanding the model complexity to include statistical confidence and broader conformational sampling.

Acknowledgements

The authors thankfully acknowledge computer resources, technical advice and support provided by Laboratorio Nacional de Supercómputo del Sureste de México (LNS), member of the CONAHCyT Nacional Laboratories Group, with project No. 202401029N, as well as the Consejo Nacional de Humanidades, Ciencias y Tecnologías (CONAHCYT) for the scholarship awarded to De La Rosa-Montelongo Erik (CVU 1241662).

References

1. Scuderi, C.; De Filippis, D.; Iuvone, T.; Blasio, A.; Steardo, A.; Esposito, G. *Phytother. Res.* **2009** *23*, 597–602. DOI: https://doi.org/10.1002/ptr.2625.
2. Seltzer, E. S.; Watters, A. K.; MacKenzie, D.; Granat, L. M.; Zhang, D. *Cancers.* **2020** *12*, 3203. DOI: https://doi.org/10.3390/cancers12113203.
3. Peng, J.; Fan, M.; An, C.; Ni, F.; Huang, W.; Luo, J. *Basic Clin. Pharmacol. Toxicol.* **2022** *130*, 439–456. DOI: https://doi.org/10.1111/bcpt.13710.
4. Francke, N. M.; Schneider, F.; Baumann, K.; Bunjes, H. *Molecules.* **2021** *26*, 1469. DOI: https://doi.org/10.3390/molecules26051469.
5. Grifoni, L.; Vanti, G.; Donato, R.; Sacco, C.; Bilia, A. R. *Molecules.* **2022** *27*. DOI: https://doi.org/10.3390/molecules27186070.
6. Wang, C.; Cui, B.; Sun, Y.; Wang, C.; Guo, M. *LWT.* **2022** *162*, 113466. DOI: https://doi.org/10.1016/j.lwt.2022.113466.
7. Noreen, S.; et al. *Drug Deliv. Transl. Res.* **2022** *12*, 2649–2666. DOI: https://doi.org/10.1007/s13346-022-01152-3.
8. Villate, A.; San Nicolas, M.; Olivares, M.; Aizpurua-Olaizola, O.; Usobiaga, A. *Pharmaceutics.* **2023** *15*, 859. DOI: https://doi.org/10.3390/pharmaceutics15030859.
9. Plazinski, W.; Plazinska, A. *New J. Chem.* **2011** *35*, 1607. DOI: https://doi.org/10.1039/C1NJ20273A.
10. Perić-Hassler, L.; Hünenberger, P. H. *Mol. Simul.* **2010** *36*, 778–795. DOI: https://doi.org/10.1080/08927021003752853.

J. Mex. Chem. Soc. **2026**, *70(1):e2440*
Regular Issue

ISSN-e 2594-0317

11. da Silva, A. J.; dos Santos, E. S. *Eur. Biophys. J.* **2020** *49*, 571–589. DOI: https://doi.org/10.1007/s00249-020-01463-8.
12. Hollingsworth, S. A.; Dror, R. O. *Neuron.* **2018** *99*, 1129–1143. DOI: https://doi.org/10.1016/j.neuron.2018.08.011.
13. Fleten, K. G.; et al. *Mar. Drugs.* **2022** *20*, 744. DOI: https://doi.org/10.3390/md20120744.
14. Hecht, H.; Srebnik, S. *Biomacromolecules.* **2016** *17*, 2160–2167. DOI: https://doi.org/10.1021/acs.biomac.6b00378.
15. Xiang, Y.; Liu, Y.; Mi, B.; Leng, Y. *Langmuir.* **2014** *30*, 9098–9106. DOI: https://doi.org/10.1021/la501811d.
16. Hanwell, M. D.; Curtis, D. E.; Lonie, D. C.; Vandermeersch, T.; Zurek, E.; Hutchison, G. R. *J. Cheminform.* **2012** *4*, 17. DOI: https://doi.org/10.1186/1758-2946-4-17.
17. O'Boyle, N. M.; Banck, M.; James, C. A.; Morley, C.; Vandermeersch, T.; Hutchison, G. R. *J. Cheminform.* **2011** *3*, 33. DOI: https://doi.org/10.1186/1758-2946-3-33.
18. Dodda, L. S.; Cabeza de Vaca, I.; Tirado-Rives, J.; Jorgensen, W. L. *Nucleic Acids Res.* **2017** *45*, W331–W336. DOI: https://doi.org/10.1093/nar/gkx312.
19. Dodda, L. S.; Vilseck, J. Z.; Tirado-Rives, J.; Jorgensen, W. L. *J. Phys. Chem. B* **2017** *121*, 3864–3870. DOI: https://doi.org/10.1021/acs.jpcb.7b00272.
20. Jorgensen, W. L.; Tirado-Rives, J. *Proc. Natl. Acad. Sci. U.S.A.* **2005** *102*, 6665–6670. DOI: https://doi.org/10.1073/pnas.0408037102.
21. Kony, D.; Damm, W.; Stoll, S.; Van Gunsteren, W. F. *J. Comput. Chem.* **2002** *23*, 1416–1429. DOI: https://doi.org/10.1002/jcc.10139.
22. Damm, W.; Frontera, A.; Tirado-Rives, J.; Jorgensen, W. L. *J. Comput. Chem.* **1997** *18*, 1955–1970. DOI: https://doi.org/10.1002/(SICI)1096-987X(199712)18:16<1955::AID-JCC1>3.0.CO;2-L.
23. Eberhardt, J.; Santos-Martins, D.; Tillack, A. F.; Forli, S. *J. Chem. Inf. Model.* **2021** *61*, 3891–3898. DOI: https://doi.org/10.1021/acs.jcim.1c00203.
24. Trott, O.; Olson, A. J. *J. Comput. Chem.* **2010** *31*, 455–461. DOI: https://doi.org/10.1002/jcc.21334.
25. Abraham, M.; et al. *GROMACS 2023.1 Manual.* **2023**.
26. Bussi, G.; Donadio, D.; Parrinello, M. *J. Chem. Phys.* **2007** *126*. DOI: https://doi.org/10.1063/1.2408420.
27. Hess, B.; Bekker, H.; Berendsen, H. J. C.; Fraaije, J. G. E. M. *J. Comput. Chem.* **1997** *18*, 1463–1472. DOI: https://doi.org/10.1002/(SICI)1096-987X(199709)18:12<1463::AID-JCC4>3.0.CO;2-H.
28. Majimbi, M.; et al. *PLoS One.* **2021** *16*, e0243858. DOI: https://doi.org/10.1371/journal.pone.0243858.